Available online at www.sciencedirect.com
SCIENCE DIRECT
ELSEVIER
European Journal of Mechanics B/Fluids 25 (2006) 337–347
EUROPEAN JOURNAL OF MECHANICS B/FLUIDS

Optimization of the rod chain model to simulate the motions of a long flexible fiber in simple shear flows

Gang Wang, Wei Yu, Chixing Zhou *

School of Chemistry and Chemical Technology, Shanghai Jiao Tong University, Shanghai 200240, China

Received 3 November 2004; received in revised form 8 September 2005; accepted 12 September 2005

Available online 26 October 2005

Abstract

A rod-chain model was used to study the dynamics of a long flexible fiber which is suspended in a Newtonian fluid. It was shown that the fiber exhibited different apparent flexibility, which depended on the stiffness of the fiber, the strength of the flow field and the initial configuration of the fiber. Different combinations of rod length and rod number were used to simulate the motions of a long fiber in simple shear flow. Long rods would greatly save the computational resources with the loss of accuracy, while short rods would generate accurate results with the loss of efficiency. An optimum rod length was suggested to balance the requirement of accuracy and efficiency, and it was the function of the relative strength of flow field and the initial angle between fiber and vortex axis.

Keywords: Long fiber; Flexibility; Rod-chain; Numerical simulation

1. Introduction

The fibers will translate, rotate, bend and break in the processing of fiber-reinforced composites. The consequential configurations of fibers play a significant role in such properties as the elastic modulus, the thermal and electrical conductivity, and the thermal expansivity. There have already been many investigations on short fiber suspensions, and some models have already been utilized in commercial software. However, it is not easy to simulate the morphology of long fibers in suspensions, especially in concentrated systems which are the common cases in industry. The most difficulties with the long fibers come from its most significant property, the flexibility. The "apparent" flexibility of the fiber may vary with the properties of the fiber, the strength of the flow field and furthermore the configuration of the fiber. Arlov and his co-workers [1] classified the dynamics of flexible fibers into three modes: "flexible spin", "flexible spin-rotation" and some other configurations when the fiber is extremely flexible, such as "springy rotations", "snake turn" and "S-turns". The different dynamics of long fibers reflects the relative flexibility of fiber under different circumstances.

During the last decades, some useful methods had been suggested to numerically simulate the dynamics of long fibers. Yamamoto et al. [2–6] regarded a fiber as a group of beads that are lined up and bonded to each neighbor (named

* Corresponding author. Tel.: +86 21 5474 3275; fax: +86 21 5474 1297.
E-mail address: cxzhou@sjtu.edu.cn (C. Zhou).

0997-7546/$ – see front matter
doi:10.1016/j.euromechflu.2005.09.004

as bead-chain). Each pair of bonded spheres can stretch, bend and twist. The rigidity or flexibility of fibers varies with the strengths of stretch, bend or twist. The dynamic behavior of fibers in a flow field can then be determined by solving a group of translational and rotational equations for individual spheres. The bead-chain model shows great advantages in precisely capturing the moving path of every point on the fiber. Therefore, it was believed to be the most suitable assumption to obtain the most accurate dynamics of a flexible long fiber. However, the bead-chain model starts to show its deficiency when the fiber is relatively long since the equations from the requirement of chain connectivity must be solved iteratively and simultaneously with the equation of motion. The CPU-time of bead-chain algorithm is $O(N_b^3)$ for small N_b and $O(N_b^4)$ for large N_b [7] (N_b is the number of beads in a fiber). Enormously high cost of computational resources restrict the application of such model to the suspension consisted of long fibers and polymers.

To overcome such restrictions, a kind of "coarse-grained" procedure was taken to combine several beads into a basic element. On the basis of Brownian dynamical (BD) simulations of needle chains in macromolecular simulations, Skjetne et al. [7–14] discretized the fiber into several rigid needle elements connected by the ball and socket (named as needle-chain). The rigid needle can be prolate spheroid [8], cylindrical rod [7,10,13,14] or spherical beads [9,11,12]. The needle-chain algorithm proves to be more efficient, and the computational cost is reduced to $O(N_f^2)$ (N_f is the number of needles in a fiber). Tang and Advani modeled flexible fibers as sphere chains linked by rigid rods and ball-socket joints, and they simulated the dynamics and viscosity of flexible fiber suspensions with several predefined unit rods and joints, where the fibers have aspect ratios near 20. Although the simulated results agreed with experiments well, the number and length of rods still need to be defined before simulation [15]. According to the results of these researches, the needle-chain model can greatly save the computational time of long fibers. However, it is believed that too long needle length will greatly reduce the accuracy of the simulation for a relatively flexible fiber. Forgacs and Manson [16] found that there is a critical value of shear stress (velocity gradient × viscosity) at which the shear-induced axial compression causes the fiber to buckle. The shape of a fiber will become complicated if it is several times longer than the critical buckle length. In the needle chain simulations, the aspect ratio of the rigid needle varies from 1∼3 [7–12] to 5∼30 [13,14]. All these needle lengths were chosen in an arbitrary manner. Too long needle length would probably induce unexpected large errors in the dynamics of a long fiber. However, no such conclusions exist yet about the optimum needle length that can balance the computational resources and the computational precision.

In this paper, we performed numerical simulations on the motions of a flexible fiber with different combinations of the rod length and the rod number. Our aim is to find the most suitable length of the rod in the simulations of long fibers. A brief description of the model is given in Section 2 and in Section 3 the numerical results and discussions are presented. Section 4 summarizes the results of the simulations.

2. Model

In this simulation, the flexible fiber is assumed to be composed by a chain of several rigid rods. Each rod is further assumed to be a series of beads which are connected each other and aligned in a straight line. Such assumption facilitates the calculation of the hydrodynamic forces and torques on the rod. The configuration of a long flexible fiber is schematically shown in Fig. 1. Conceptually, this is similar to the needle-chain model that has been used by Skjetne et al. [7–10] and the rod-chain model by Schmid et al. [13] and Switzer et al. [14]. The main differences lie in the determination of the internal constraint forces between the neighbor rods. Furthermore, they all neglected particle

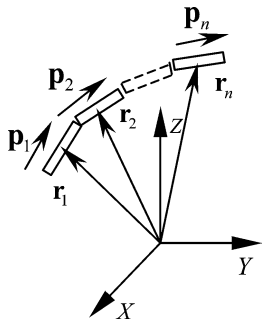

Fig. 1. The schematics of a fiber with a rod-chain and a rod with a bead-chain.

inertias. However, we think it is not suitable to neglect the inertias of different rods in such simulations. Therefore, we kept the inertia and followed the way which was adopted by Yamamoto [2–6].

The main conditions imposed in this paper are:

- The suspension is a Newtonian fluid.
- The Brownian motion is neglected.
- The velocity gradients can not be disturbed by the motion of fiber.
- The de-coupling of flow and fiber orientation is valid.
- Rods and fibers are force and torque free at all times and fibers are inextensible.

In the model descriptions below, all the quantities and equations are expressed in the dimensionless form. The time t, the length of rod l, the force $\boldsymbol{F}$ and the torque $\boldsymbol{T}$ are nondimensionalized respectively as below,

$$\hat{t} = t\dot{\gamma}, \tag{1a}$$

$$\hat{l} = l/a, \tag{1b}$$

$$\widehat{\boldsymbol{F}} = \boldsymbol{F}/\pi\eta a^2\dot{\gamma}, \tag{1c}$$

$$\widehat{\boldsymbol{T}} = \boldsymbol{T}/\pi\eta a^3\dot{\gamma}, \tag{1d}$$

where a is the radius of fiber, η is the bulk viscosity, $\dot{\gamma} = \sqrt{2\,\mathrm{tr}\,\boldsymbol{D}^2}$ is the shear rate, D is the deformation rate tensor defined as $D = \frac{1}{2}(\boldsymbol{\kappa} + \boldsymbol{\kappa}^{\mathrm{T}})$, $\boldsymbol{\kappa}$ is the velocity gradient tensor. We will omit "$\hat{}$" in the following sections and all the quantities are dimensionless if not otherwise stated.

Assume a fiber with aspect ratio r_e is composed of N_f rods numbered from 1 on one end to N_f on the other. The length of each rod is l, and each rod is composed of N beads. Since free draining approximation for polymer dynamics is used, the hydrodynamic force exerted on a bead is assumed to be proportional to the relative velocity of the bead with the macroscopic flow. Let $\boldsymbol{r}_i$ and $\boldsymbol{p}_i$ be the central position and direction vectors of rod i, the hydrodynamic friction force acting on mass center of rod i is,

$$\boldsymbol{F}_i^{\mathrm{h}} = 6N(\boldsymbol{\kappa}\cdot\boldsymbol{r}_i - \boldsymbol{v}_i), \quad i = 1 \sim N_f, \tag{2}$$

where $\boldsymbol{v}_i$ is the velocity of center of rod i.

Likewise, the angular friction torque can be expressed as [16,17],

$$\boldsymbol{T}_i^{\mathrm{h}} = -2N^3(\boldsymbol{\omega}_i - \boldsymbol{\omega}_i^{\infty}), \quad i = 1 \sim N_f, \tag{3}$$

where $\boldsymbol{\omega}_i$ is the angular velocity of rod i, $\boldsymbol{\omega}_i^{\infty}$ is the bulk angular velocity of the corresponding position.

The bending torque $\boldsymbol{T}^{\mathrm{b}}$ between two neighbor rods is assumed to be proportional to the difference between the bending angle θ^{b} and their equilibrium value [9],

$$\boldsymbol{T}_i^{\mathrm{b}} = -k^{\mathrm{b}}(\theta^{\mathrm{b}} - \theta_{\mathrm{eq}}^{\mathrm{b}})\boldsymbol{n}_i^{\mathrm{b}}, \quad i = 1 \sim N_f, \tag{4}$$

where $\boldsymbol{n}_i^{\mathrm{b}} = (\boldsymbol{p}_i \times \boldsymbol{p}_{i+1})/|\boldsymbol{p}_i \times \boldsymbol{p}_{i+1}|$ is the unit vector normal to the plane of bending, and $\theta^{\mathrm{b}} = \cos^{-1}[(\boldsymbol{p}_i \cdot \boldsymbol{p}_{i+1})/|\boldsymbol{p}_i \cdot \boldsymbol{p}_{i+1}|]$. The bending constant k^{b} is related to the bending stiffness of the fiber for small deformation via $k^{\mathrm{b}} = EI^{\mathrm{b}}/(2Na)$, where E is the Young's modulus, $I^{\mathrm{b}} = \pi a^4/4$ is the rotational inertia moment.

The twisting torque $\boldsymbol{T}^{\mathrm{t}}$ is defined in terms of the twist angle θ^{t} between two contiguous rods [9],

$$\boldsymbol{T}_i^{\mathrm{t}} = -k^{\mathrm{t}}(\theta^{\mathrm{t}} - \theta_{\mathrm{eq}}^{\mathrm{t}})\boldsymbol{p}_{i+1}, \quad i = 1 \sim N_f. \tag{5}$$

In order to determine the twist angle, a body-fixed unit vector $\mathbf{u}_i$ perpendicular to rod i is used, $\theta^{\mathrm{t}} = \cos^{-1}[(\mathbf{u}_i \cdot \mathbf{u}'_{i+1})/|\mathbf{u}'_{i+1}|]$, where $\mathbf{u}'_{i+1} = \mathbf{u}_i - (\mathbf{u}_i \cdot \boldsymbol{p}_{i+1})\boldsymbol{p}_{i+1}$. The torsion constant for small deformations is $k^{\mathrm{t}} = GI^{\mathrm{t}}/(2a)$, G is the shear modulus, $I^{\mathrm{t}} = \pi a^4/2$ is the polar inertia moment. For a straight fiber which used in this research, $\theta_{\mathrm{eq}}^{\mathrm{b}} = 0$ and $\theta_{\mathrm{eq}}^{\mathrm{t}} = 0$.

There are some other forces can not be solved directly, which can be summed to an internal constraint force $\boldsymbol{X}$. For a fiber with N_f rods, there are $N_f + 1$ ends of rods. We take $\boldsymbol{X}_0$ and $\boldsymbol{X}_{N_f}$ as the constraint forces at fiber ends, and $\boldsymbol{X}_i$ $(i = 1 \sim N_f - 1)$ is the internal constraint forces. It can be solved by the following method [2–6].

The motion of rod i satisfies:

$$\pi a^2 l\rho \frac{\mathrm{d}\boldsymbol{v}_i}{\mathrm{d}t} = \boldsymbol{F}_i^{\mathrm{h}} + \boldsymbol{X}_i - \boldsymbol{X}_{i+1}, \quad i = 1 \sim N_f. \tag{6}$$

Assume the particle Reynolds number to be $Re = \pi a^2 \rho\dot{\gamma}/\eta$ (ρ is the density of the fiber), the above equation turns to dimensionless form:

$$\frac{\mathrm{d}\boldsymbol{v}_i}{\mathrm{d}t} = \frac{1}{2NRe}(\boldsymbol{F}_i^{\mathrm{h}} + \boldsymbol{X}_i - \boldsymbol{X}_{i+1}), \quad i = 1 \sim N_f. \tag{7}$$

The angular momentum balance for rod i in dimensionless form is:

$$\frac{\mathrm{d}\boldsymbol{\omega}_i}{\mathrm{d}t} = \frac{3}{2Re\,N^3}\big[\boldsymbol{T}_i^{\mathrm{h}} + \boldsymbol{T}_i^{\mathrm{b}} - \boldsymbol{T}_{i+1}^{\mathrm{b}} + \boldsymbol{T}_i^{\mathrm{t}} - \boldsymbol{T}_{i+1}^{\mathrm{t}} - N\boldsymbol{p}_i \times (\boldsymbol{X}_i + \boldsymbol{X}_{i+1})\big], \quad i = 1 \sim N_f. \tag{8}$$

The fiber should maintain continuity, namely the translational velocities of the contact point of two neighbor rods always are the same,

$$\boldsymbol{v}_i + \boldsymbol{\omega}_i \times aN\boldsymbol{p}_i = \boldsymbol{v}_{i+1} - \boldsymbol{\omega}_{i+1} \times aN\boldsymbol{p}_{i+1}, \quad i = 1 \sim N_f - 1. \tag{9}$$

Differentiate the last equation with respect to time t and make it dimensionless, we have

$$\begin{aligned}&\frac{\mathrm{d}\boldsymbol{v}_i}{\mathrm{d}t} + \frac{\mathrm{d}\boldsymbol{\omega}_i}{\mathrm{d}t} \times N\boldsymbol{p}_i + \boldsymbol{\omega}_i \times N(\boldsymbol{\omega}_i \times \boldsymbol{p}_i) = \frac{\mathrm{d}\boldsymbol{v}_{i+1}}{\mathrm{d}t} - \frac{\mathrm{d}\boldsymbol{\omega}_{i+1}}{\mathrm{d}t} \times N\boldsymbol{p}_{i+1} - \boldsymbol{\omega}_{i+1} \times N(\boldsymbol{\omega}_{i+1} \times \boldsymbol{p}_{i+1}),\\ &\quad i = 1 \sim N_f - 1.\end{aligned} \tag{10}$$

Substitute Eqs. (7) and (8) into (10) using the translational velocity and the angular velocity at time t, we obtain the equations for the internal constraint $\boldsymbol{X}$,

$$\begin{aligned}&(\boldsymbol{X}_i - 2\boldsymbol{X}_{i+1} + \boldsymbol{X}_{i+2}) - 3\big[\boldsymbol{p}_i \times (\boldsymbol{X}_i + \boldsymbol{X}_{i+1}) \times \boldsymbol{p}_i + \boldsymbol{p}_{i+1} \times (\boldsymbol{X}_{i+1} + \boldsymbol{X}_{i+2}) \times \boldsymbol{p}_{i+1}\big]\\ &\quad = (\boldsymbol{F}_{i+1}^{\mathrm{h}} - \boldsymbol{F}_i^{\mathrm{h}}) - \frac{3}{N}\big[(\boldsymbol{T}_i^{\mathrm{h}} + \boldsymbol{T}_i^{\mathrm{b}} - \boldsymbol{T}_{i+1}^{\mathrm{b}}) \times \boldsymbol{p}_i + (\boldsymbol{T}_{i+1}^{\mathrm{h}} + \boldsymbol{T}_{i+1}^{\mathrm{b}} - \boldsymbol{T}_{i+2}^{\mathrm{b}}) \times \boldsymbol{p}_{i+1}\big]\\ &\qquad - 2ReN^2\big[\boldsymbol{\omega}_i \times (\boldsymbol{\omega}_i \times \boldsymbol{p}_i) + \boldsymbol{\omega}_{i+1} \times (\boldsymbol{\omega}_{i+1} \times \boldsymbol{p}_{i+1})\big], \quad i = 1 \sim N_f - 1.\end{aligned} \tag{11}$$

When obtaining Eq. (11), such assumptions has been made that the internal forces at fiber ends are free, i.e. $\boldsymbol{X}_0$ and $\boldsymbol{X}_{N_f}$ are zeros. Therefore, these equations are enough to solve the $N_f - 1$ unknown internal constraints. Then they can be used to solve angular velocities of each rod at corresponding timestep.

The trajectory of barycenter of a uniformly fiber obeys:

$$\boldsymbol{r}_m^{\mathrm{t}} = \boldsymbol{r}_m^{t-1} + \Delta t \sum \boldsymbol{v}_i^{t-1}/N_f, \tag{12}$$

where $\boldsymbol{r}_m$ is the center of mass of the fiber.

The dynamics of the rods are determined by the following procedure:

a. At $t = 0$, an initialize configuration of fiber and a flow field is given. Generally the fiber is stationary at the beginning.
b. Solve the hydrodynamic friction forces ($\boldsymbol{F}^{\mathrm{h}}$) and torques ($\boldsymbol{T}^{\mathrm{h}}$), bending and torsion torques ($\boldsymbol{T}^{\mathrm{b}}$ and $\boldsymbol{T}^{\mathrm{t}}$) on rods from Eqs. (2)–(5) at time t.
c. Solve the internal constraint forces ($\boldsymbol{X}$) from Eq. (11).
d. Use $\boldsymbol{X}$ to update the angular velocity ($\boldsymbol{\omega}$) of rods at $t + \Delta t$ from Eq. (8) by the explicit Euler method.
e. Determine the center ($\boldsymbol{r}_m$) of the fiber by means of the old translational velocity $\boldsymbol{v}^{t-1}$ use Eq. (12), then the new direction ($\boldsymbol{p}_i$) and position ($\boldsymbol{r}_i$) at next step.

$$\boldsymbol{p}_i = \frac{\boldsymbol{p}_i^{t-1} + \boldsymbol{\omega}_i \times \boldsymbol{p}_i^{t-1}\Delta t}{|\boldsymbol{p}_i^{t-1} + \boldsymbol{\omega}_i \times \boldsymbol{p}_i^{t-1}\Delta t|}, \quad i = 1 \sim N_f. \tag{13}$$

If there were odd rods, the positions were:

$$\boldsymbol{r}_{(N_f+1)/2} = \boldsymbol{r}_m \quad \text{and} \quad \boldsymbol{r}_i = \boldsymbol{r}_m + N \sum_{n=(N_f+1)/2+1}^{i} (\boldsymbol{p}_{n-1} + \boldsymbol{p}_n), \quad i = \frac{N_f + 1}{2} + 1 \sim N_f,$$

and

$$\boldsymbol{r}_i = \boldsymbol{r}_m - N \sum_{n=(N_f+1)/2-1}^{i} (\boldsymbol{p}_n + \boldsymbol{p}_{n+1}), \quad i = \frac{N_f+1}{2} - 1 \sim 1. \tag{14-1}$$

If there were even rods, the positions were:

$$\boldsymbol{r}_{N_f/2+1} = \boldsymbol{r}_m + N\boldsymbol{p}_{N_f/2+1}, \quad \text{and} \quad \boldsymbol{r}_i = \boldsymbol{r}_{N_f/2+1} + N \sum_{n=N_f/2+2}^{i} (\boldsymbol{p}_{n-1} + \boldsymbol{p}_n), \quad i = \frac{N_f}{2} + 2 \sim N_f,$$

and

$$\boldsymbol{r}_{N_f/2} = \boldsymbol{r}_m - N\boldsymbol{p}_{N_f/2}, \quad \text{and} \quad \boldsymbol{r}_i = \boldsymbol{r}_{N_f/2} - N \sum_{n=N_f/2-1}^{i} (\boldsymbol{p}_n + \boldsymbol{p}_{n+1}), \quad i = \frac{N_f}{2} - 1 \sim 1. \tag{14-2}$$

f. Get the translational velocity of rods, $\boldsymbol{v}_i = (\boldsymbol{r}_i - \boldsymbol{r}_i^{t-1})/\Delta t$.
g. Repeat steps from (b) to (f), we obtain the motions of each rod, and then we can prescribe the motions of the fiber.

It is true that a fiber may cut cross itself if the fiber is sufficient flexible (which means that the fiber must be long enough under a constant modulus). The morphology of a fiber in flow field will be much complicated if this happens. However, most researchers including us neglect this possibility in their computations [2–14]. In fact, to avoid this complicated situation, we limit the fiber length in this study to be less than 50, which in turn no cut cross in a flexible fiber occurs in our computations.

3. Result and discussion

Forgacs et al. [16] reported that the axial force along a fiber is proportional to the length of the fiber. The force turns stronger when the fiber becomes longer. The fiber bends if the force exceeds the fiber's strength. They also pointed out that there is a critical buckle aspect ratio of a fiber above which the fiber will be bent. The relationship between the relative strength of flow ($\eta\dot{\gamma}/E$) and the critical buckle aspect ratio (r_c) was proposed [16]:

$$\frac{\eta\dot{\gamma}}{E} = \frac{\ln(2r_c) - 1.75}{2r_c^4}. \tag{15}$$

For example, when $E/\eta\dot{\gamma} = 2 \times 10^5$, $r_c = 21.13$.

Reynolds number used in this work is 0.1 since the simulation results are same when it is less than 0.1 but needs shorter time step size and longer computation time. The corresponding time step size used is $\Delta t = 0.001$. All simulations reported in this work were carried out on a PC with one AMD 1600 + MHz processor, and a main memory size of 512 M bytes. It takes several minutes to about an hour for 100,000 time steps depending on the segments number of a fiber.

3.1. Verification of the model

It is necessary to verify the validity of this simulation firstly for rigid and flexible fiber with pre-researchers before investigating the effect of the rod length on the simulation results. Several simulation results were presented to compare with the theoretical results of a rigid fiber by Jeffery theory and the numerical results of a flexible fiber by Skjetne et al. [9] and Fan et al. [11].

3.1.1. Rigid fibers

Jeffery [18] predicted theoretically that the major axis of a prolate spheroid of axis ratio r_e should execute a spherical elliptical orbit when it rotates in a viscous fluid. The orbit constant C, $C = \tan\theta\sqrt{\cos^2\phi + \sin^2\phi/r_e^2}$, is related to the eccentricity of the path described by the ends of the particle axis. The particle rotates entirely in the X–Y plane as $C \to \infty$. The relationship between C, X, Y, Z axes and initial angles θ, ϕ is shown in Fig. 2. X axis is the flow direction, Y axis is the direction of velocity gradient, and Z axis is the direction of vorticity.

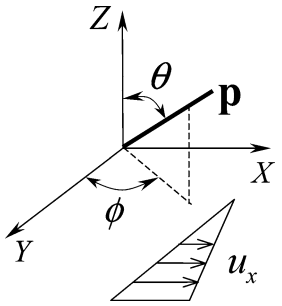

Fig. 2. The schematic picture of a fiber in the simple shear flow field.

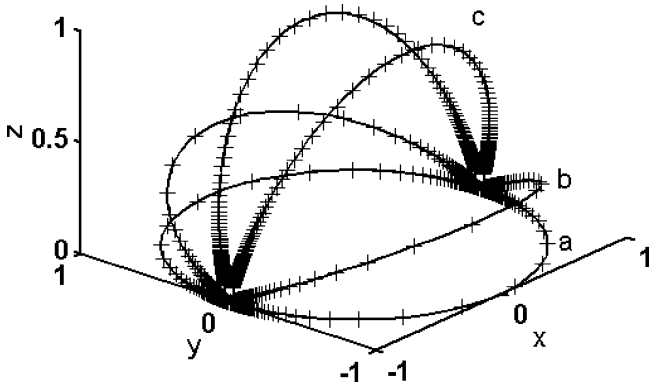

Fig. 3. The orbits of a rigid fiber ($r_e = 20$, $r_c \approx 21.13$), "+" are simulated results, real lines are Jeffery orbits, a: $C = \infty$, b: $C = 0.36$, c: $C = 1.73$.

For a fiber with aspect ratio 20 floats in a fluid with $E/\eta\dot{\gamma} = 2 \times 10^5$, the fiber will translate and rotate just like a rigid one, and no bending appears since its length is shorter than the critical value. Under such conditions, we discretize the fiber into several different combinations of N_f and N, such as 20×1, 10×2, 5×4. The results of different combinations exhibit almost the same orbit and the fiber behaves like a rigid body (the end-to-end distance changed less than 0.01% in a period). These results prove that different combinations of N_f and N have little effects on the orbits of fiber end. The orbits from the simulations and comparisons with Jeffery's theory are displayed in Fig. 3. Exact matches between the simulation results and Jeffery's theory confirm the validity of our simulations for single rigid fiber.

3.1.2. Flexible fibers

When a fiber's aspect ratio exceeds the critical buckle ratio, the fiber becomes easier to deform under the hydrodynamic force. The dynamics of the suspension system composed of such fibers and a Newtonian fluid become more complicated. We know that a rigid fiber rotates in a stable orbit and the orbit constant changes from 0 to ∞ for a fiber parallel to the vortex axis or the X–Y plane, while the end of a flexible fiber does not follow a stable orbit as a rigid one and the orbit drifts toward $C = \infty$ or $C = 0$ depending on a big C ($C > 0.2$) or a small C ($C < 0.05$) [9].

We defined the end-to-end normalized vectors of the fiber as the direction vectors, which is equivalent to the definition employed by Arlov et al. [1]. End-to-end normalized vector can be a good representation of fiber orientation if the fiber is almost straight. For curved fiber, end-to-end vector can also give an indication of fiber orientation. End-to-end vector has been used in some other cases to represent the orientation, such as the orientation of polymer chain coil in a flow field. The computed orbits of the end of vectors are presented in Fig. 4. It shows that the orbits of flexible fibers with big orbit constant drift toward X–Y plane, which is the same as the experimental results of Arlov et al. [1] and the simulation results of Skjetne et al. [7,11].

According to Forgacs et al. [13], a single long fiber floated in a simple shear flow will bend by the compressing stress of hydrodynamic force when $\phi < 0$ and straighten again by strain force at $\phi > 0$ if the fiber exceeds the critical buckle length. Such behaviors were predicted by Hinch for a flexible fiber with infinitesimal thickness and zero modulus [19]. The simulation results with our model on the deformation of a fiber with $r_e = 30$, $\dot{\gamma} = 1$ and $r_c \approx 11.15$ are showed in Fig. 5. The fiber is straightened when it is aligned with the shear flow field ($\phi > 0$), while the shape of the fiber becomes highly deformed when $\phi < 0$. They match the predictions of Hinch [19] and the results of Joung et al. [11] qualitatively well.

3.2. Flexibility of the fiber

We would find a suitable approach to choose the best rod length in the simulations. In fact, different chosen of rod length reflects the apparent flexibility of the fiber. The fiber will be more like a rigid one if the rod length is relative long, or a fiber is readily to deform if the rod length is very short. We performed some simulations on the different combinations of $N_f \times N$ for a fiber to detect the accuracy and efficiency, especially for long fibers (several times

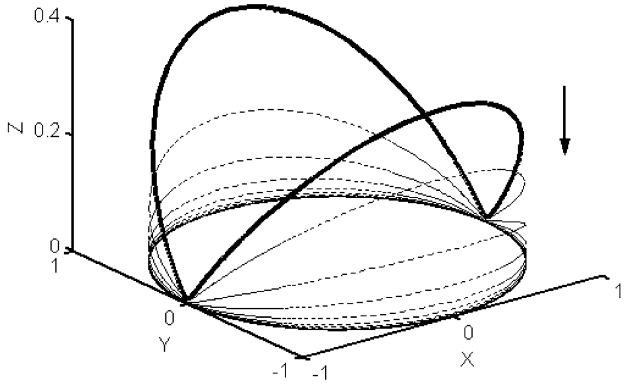

Fig. 4. Orbit drift for a flexible fiber ($r_e = 40$, $r_c \approx 11.15$, $C = 2.64$, $N_f \times N = 20 \times 2$), the bold line is the Jeffery orbit of initial condition.

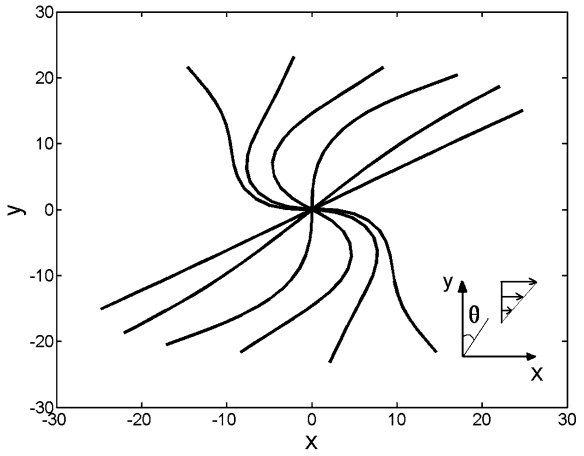

Fig. 5. Deformation of a flexible fiber in a simple shear flow, lines present the axis of fiber in different positions ($r_e = 30$, $r_c \approx 11.15$, $N_f \times N = 30 \times 1$).

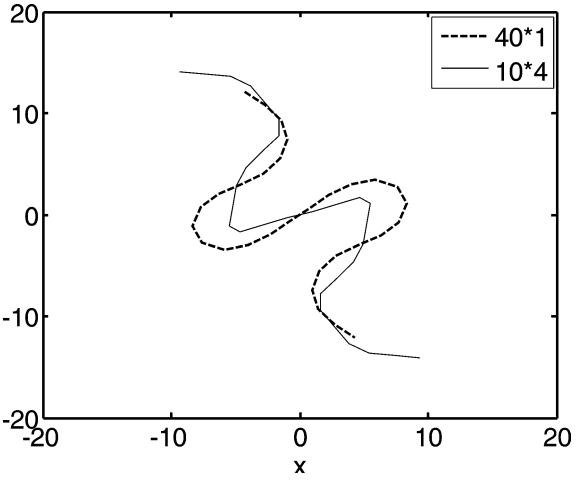

Fig. 6. Shapes of fiber axis for different rod length with $r_e = 40$, $r_c \approx 10.70$.

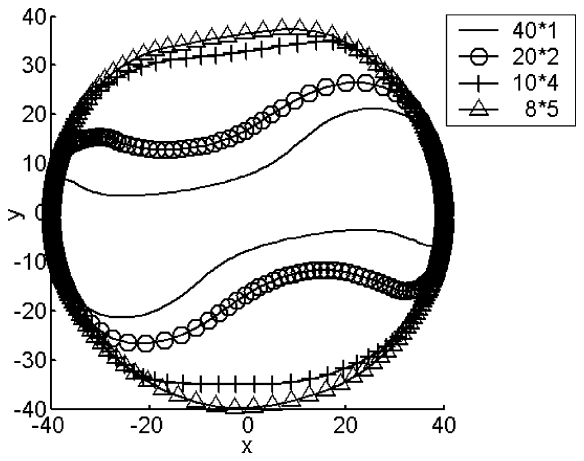

Fig. 7. Trajectories of one end of a fiber for different combinations with $r_e = 40$, $r_c \approx 10.70$.

longer than the critical buckle value). The computation result of the bead-chain model will be used as a reference for comparison.

3.2.1. Effect of the rod length

When the fiber length is less than the critical buckle value, the fiber always keeps straight during translation and rotation, and there are very little differences among the results of different combinations for such a fiber, such as 20×1, 10×2 and 5×4, 4×5. When the fiber length exceeds the critical buckle value, the results is totally different as discussed above. Therefore, we will focus on the behavior of long flexible fibers suspended in the shear flow field here. Considering a fiber with aspect ratio 40 lying in X–Y plane, assuming the ratio of Young's modulus to shear stress $E/\eta\dot{\gamma} = 2 \times 10^4$, the critical buckle aspect ratio will be 10.70 according to Eq. (15), indicating that such a long fiber is highly deformable.

Fig. 6 shows different bending shapes of a fiber of $r_e = 40$ with 40×1 and 10×4 combinations. It is found that the curve with 10×4 is not as smooth as one with 40×1, and former shows some sharp corners along the line although they have same deformation period. It seems that the fiber with long rods behaves stiffer than the one with short ones. Then, we adopted four different combinations such as 40×1, 20×2, 10×4 and 8×5 in the computations to further check the effect of the rod length. The results are presented in Fig. 7. It is found that the area occupied by a fiber

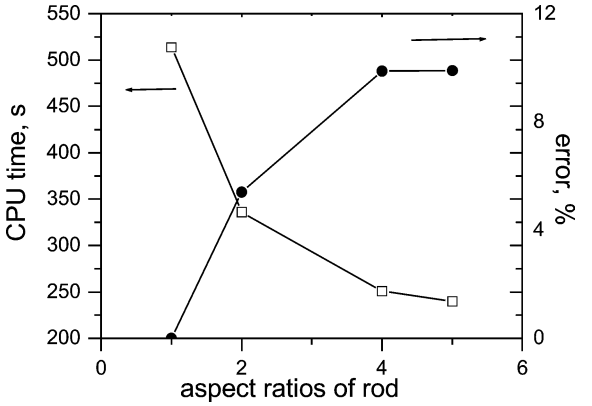

Fig. 8. Computational time and relative errors under different combinations with $r_e = 30$, $r_c \approx 11.15$.

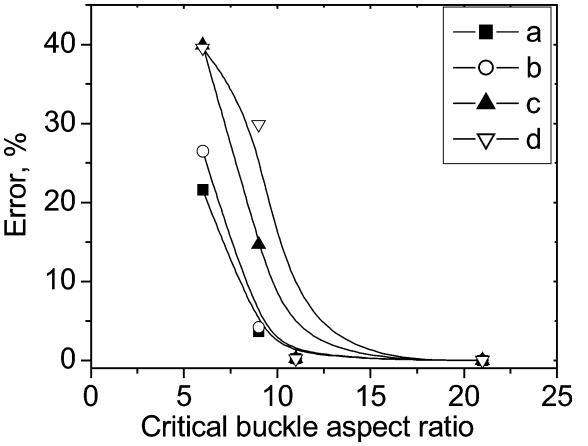

Fig. 9. Relative errors estimated with different critical buckle aspect ratios r_c with different rod length: (a) 2, (b) 3, (c) 4 and (d) 5.

during rotation became larger with longer rod. Such increase of area means the fiber with long rod can not deform as freely as the bead chain. Above results indicate that the longer the rod length, the larger the error of the simulation as compared to the bead chain model. In order to evaluate the accuracy of the simulations, we set the biggest Y value of the fiber in a rotation for $N = 1$ (the rod is reduced to a sphere) as a reference. The percentage variation of maximum Y values of other combinations is used to represent the relative accuracy. The predictions are showed in Fig. 8. It is clear that the relative errors increase greatly with the increase the rod length.

On the other hand we noted the CPU time spent for 100,000 time steps decreased quickly with longer rods according to our computational results. That indicates that long rods would greatly save the computational resources as pointed out by Skjetne et al. [7]. The effect of the aspect ratios of rod on CPU time is also represented in Fig. 8. It suggests an optimum rod length (about 2∼3) may be the best choice to balance the two demands of accuracy and efficiency.

3.2.2. Influences of several factors

We have shown that the different choice of rod length under specified flow field produce different results with varied accuracy. It is readily to understand such that the best choice of rod length should dependent on the strength of the flow field. It can be seen from Eq. (15) that large shear stress results in small critical buckle length. Therefore, the optimum rod length should be the function of the critical buckle length. Fig. 9 shows that the relative errors of simulations on a fiber with $r_e = 30$ lying in X–Y plane. It is seen that for a very "flexible" fiber (small critical buckle length), large rod element would produce unacceptable huge errors. When the apparent flexibility decreases (critical buckle length increase), even large rod length can give excellent results with negligible relative error.

The flexibility of a fiber is related to its length and environment and longer fibers behave more flexible. Fig. 10 shows the relative errors for different fibers with aspect ratios in the range of 10–50 and fibers are totally lying on the X–Y plane and the critical buckle aspect ratio is $r_c \approx 7.13$. The errors become bigger for longer fibers.

When the initial angle between fiber and vortex axis changes from $\theta = 90°$ to $\theta = 0°$, the total axial force $\boldsymbol{F}$ exerting on the central cross section of the fiber has direct proportional relationship with θ [20],

$$\boldsymbol{F} \propto \frac{\tan^2\theta}{\tan^2\theta + 1}. \tag{16}$$

The critical buckle aspect ratio changes with the initial angle θ, i.e. the flexibility of a fiber depends on the initial angle. The fiber behaves more flexible when θ is bigger. First we investigated a fiber located in initial angle $\theta = 80°$. The different combinations have little influences on the orbit period of the fiber. The total differences in the period are less than 3 seconds ($T = 160$∼162 seconds, Table 1). But there were big changes of the trajectories of fiber ends (Fig. 11). The orbit of bead chain ($N = 1$) drifts to the shear plane. The orbits of rod chains ($N \geqslant 2$) start to deviate from that of the bead chain as the rod length increase. The orbit is completely different from the bead chain when $N = 5$.

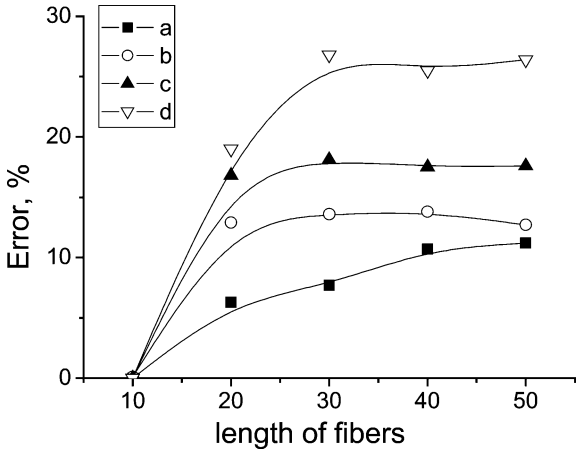

Fig. 10. Relative errors with different fiber length and (a) $N = 2$, (b) $N = 3$, (c) $N = 4$, (d) $N = 5$.

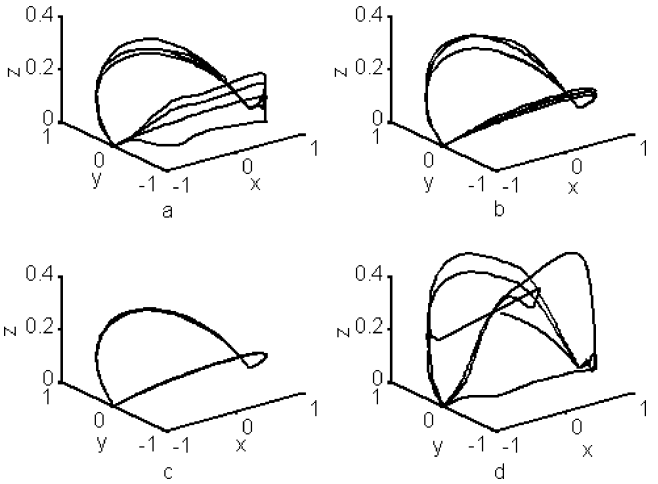

Fig. 11. Orbits of ends for a flexible fiber: $r_e = 40$, $r_c \approx 11.15$, $\theta = 80°$. (a) $N = 1$, (b) $N = 2$, (c) $N = 3$, (d) $N = 4$.

Table 1
The periods of a fiber with aspect ratio 40 located in the angle $\theta = 80°$

Rod length	1	2	3	4
Periods, s	160.51	160.58	160.90	162.13

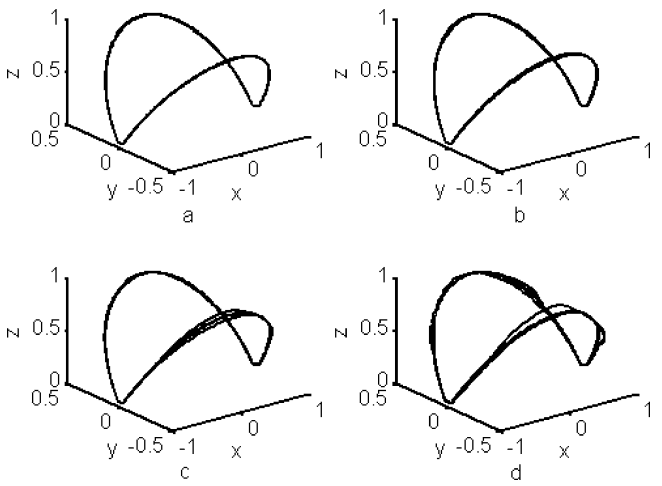

Fig. 12. Orbits of ends for a flexible fiber: $r_e = 40$, $r_c \approx 11.15$, $\theta = 30°$, (a) $N = 1$, (b) $N = 2$, (c) $N = 4$, (d) $N = 5$.

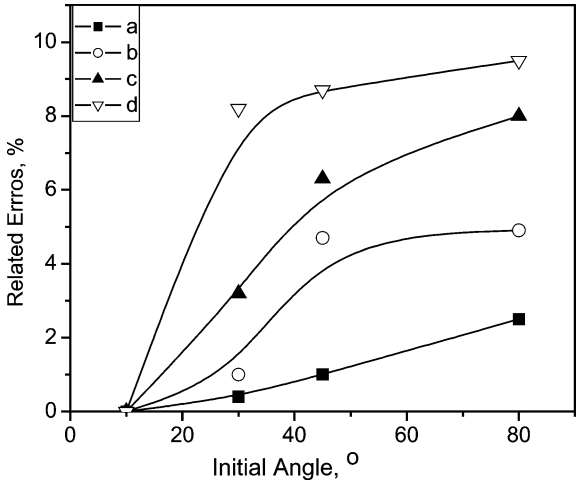

Fig. 13. Relative errors under different initial angles θ with $r_e = 30$, $r_c \approx 7.13$ at XY plane, and (a) $N = 2$, (b) $N = 3$, (c) $N = 4$, (d) $N = 5$.

Now keep the aspect ratio and the fluid field unchanged, but alter the initial angle to $\theta = 30°$. The fiber holds straight in our simulations, and followed the Jeffery orbit without drifting. The trajectories keep unchanged until the rod longer than 4 (Fig. 12). Hence it is necessary to use a small number of long rods to complete the simulation when a fiber's initial orientation is close to the vortex axis.

Fig. 13 shows the relative errors of simulations on a long fiber with $r_e = 30$ which initially locates at different angles to the vortex axis. The overall errors decrease with the increase of initial angles, and the errors decrease as the rod length increases.

Table 2
The relative errors and computational time saved in the simulations by using the optimum rod length

r_c on XY plane	Initial angles, °	$N_f \times N$	Errors, %	Time saved, %
8.60	90	13×2.31	0.054	52.7
11.15		10×3	1.13	67.1
14.69		8×3.75	1.08	77.1
7.13	30	8×3.75	1.49	77.1
	60	12×2.5	1.42	56.8
	70	14×2.14	2.59	47.9

3.2.3. An optimum rod length of the rod-chain

So when the relative flow field is weaker, or the fiber locates in a less initial angle, a longer element can be used. We fitted an equation to estimate an optimum rod length, which relies on the aspect ratio of the fiber, the critical buckle length and the initial angle,

$$N = C\frac{r_c}{r_e}\frac{\tan^2\theta + 1}{\tan^2\theta}, \quad 0 \leqslant \theta \leqslant 90^\circ,\ r_c \geqslant 6, \tag{17}$$

where C is estimated to be 8 to make the errors less than 5% in our simulations.

There are two extreme situation should be considered. One is for a rigid fiber. Long rod element can be used to conduct the simulation. For example, the optimum length can be very big when the initial angle is near $\theta = 0^\circ$, and we can use the whole fiber as a single element. The other is for an extremely flexible fiber that $N = 1$ is used as a limitation.

The relative errors of some simulations by using the optimum rod length calculated from Eq. (17) are listed in Table 2. It shows that the corresponding relative errors are within 5%, while the maximum computational time saved is over 70% where the optimum rod length varies from 1 to about 4. All the results in Table 2 suggested that we may use Eq. (17) to calculate the rod length which can reduce the computational resources without loss of the accuracy.

4. Conclusions

This paper reports a rod-chain model to simulate a flexible fiber in Newtonian fluids and the corresponding numerical results. The work focused on finding the optimum length of each rod used in the model, which highly influenced the accuracy and efficiency of simulations. An expression of such optimum length is proposed on the basis of many simulation results under different strength of flow field, different initial fiber configuration, and different combinations of the rod length and the number of rod. Simulations by using the optimum rod length prove to be of high efficiency and low relative error.

Acknowledgements

This work was supported by the National Science Foundation of China (No. 20174024 and No. 50290090).

References

[1] A.P. Arlov, O.L. Forgacs, S.G. Mason, Sven. Papperstidn. 61 (1958) 61.
[2] S. Yamamoto, T. Matsuoka, A method for dynamic simulation of rigid and flexible fibers in a flow field, J. Chem. Phys. 98 (1) (1993) 644–650.
[3] S. Yamamoto, T. Matsuoka, Viscosity of dilute suspensions of rodlike particles: a numerical simulation method, J. Chem. Phys. 100 (4) (1994) 3317–3324.
[4] S. Yamamoto, T. Matsuoka, Dynamic simulation of flow-induced fiber fracture, Polym. Engrg. Sci. 35 (12) (1995) 1022–1030.
[5] S. Yamamoto, T. Matsuoka, Dynamic simulation of fiber suspensions in shear flow, J. Chem. Phys. 102 (5) (1995) 2254–2260.
[6] S. Yamamoto, T. Matsuoka, Dynamic simulation of microstructure and rheology of fiber suspension, Polym. Engrg. Sci. 36 (19) (1996) 2396–2403.
[7] G.H. Nyland, P. Skjetne, A. Mikkelsen, A. Elgsaeter, Brownian dynamics simulation of needle chains, J. Chem. Phys. 105 (3) (1996) 1198–1207.

[8] R.F. Ross, D.J. Klingenberg, Dynamic simulation of flexible fibers composed of linked rigid bodies, J. Chem. Phys. 106 (7) (1997) 2949–2960.
[9] P. Skjetne, R.F. Ross, D.J. Klingenberg, Simulation of single fiber dynamics, J. Chem. Phys. 107 (6) (1997) 2108–2121.
[10] P. Skjetne, A. Elgsaeter, Implementation and performance of the needle chain-algorithm for Brownian dynamics simulation, Comput. Theoret. Poly. Sci. 9 (1999) 153–164.
[11] C.F. Schmid, L.H. Switzer, D.J. Klingenberg, Simulations of fiber flocculation: Effects of fiber properties and interfiber friction, J. Rheol. 44 (2000) 781–809.
[12] L.H. Switzer, D.J. Klingenberg, Rheology of sheared flexible fiber suspensions via fiber-level simulations, J. Rheol. 47 (2003) 759–778.
[13] C.G. Joung, N. Phan-Thien, X.J. Fan, Direct simulation of flexible fibers, J. Non-Newtonian Fluid Mech. 99 (2001) 1–36.
[14] C.G. Joung, N. Phan-Thien, X.J. Fan, Viscosity of curved fibers in suspension, J. Non-Newtonian Fluid Mech. 102 (2002) 1–17.
[15] W.Z. Tang, S.G. Advani, Dynamic simulation of long flexible fibers in shear flow, CMES 8 (2) (2005) 165–176.
[16] O.L. Forgacs, S.G. Mason, Particle motions in sheared suspensions IX. Spin and deformation of threadlike particles, J. Colloid Sci. 14 (1959) 457–472.
[17] M. Doi, S.F. Edwards, The Theory of Polymer Dynamics, Oxford University Press, New York, 1986 (Chapter 8).
[18] G. Jeffery, The motion of ellipsoidal particles immersed in viscous fluid, Proc. Roy Soc. Ser. A 102 (1923) 161.
[19] E.J. Hinch, The distortion of a flexible inextensible thread in a shearing flow, J. Fluid Mech. 74 (1976) 317.
[20] J.M. Burgers, Second Report on Viscosity and Plasticity, North-Holland, Amsterdam, 1938 (Chapter 3, pp. 19 and 10).